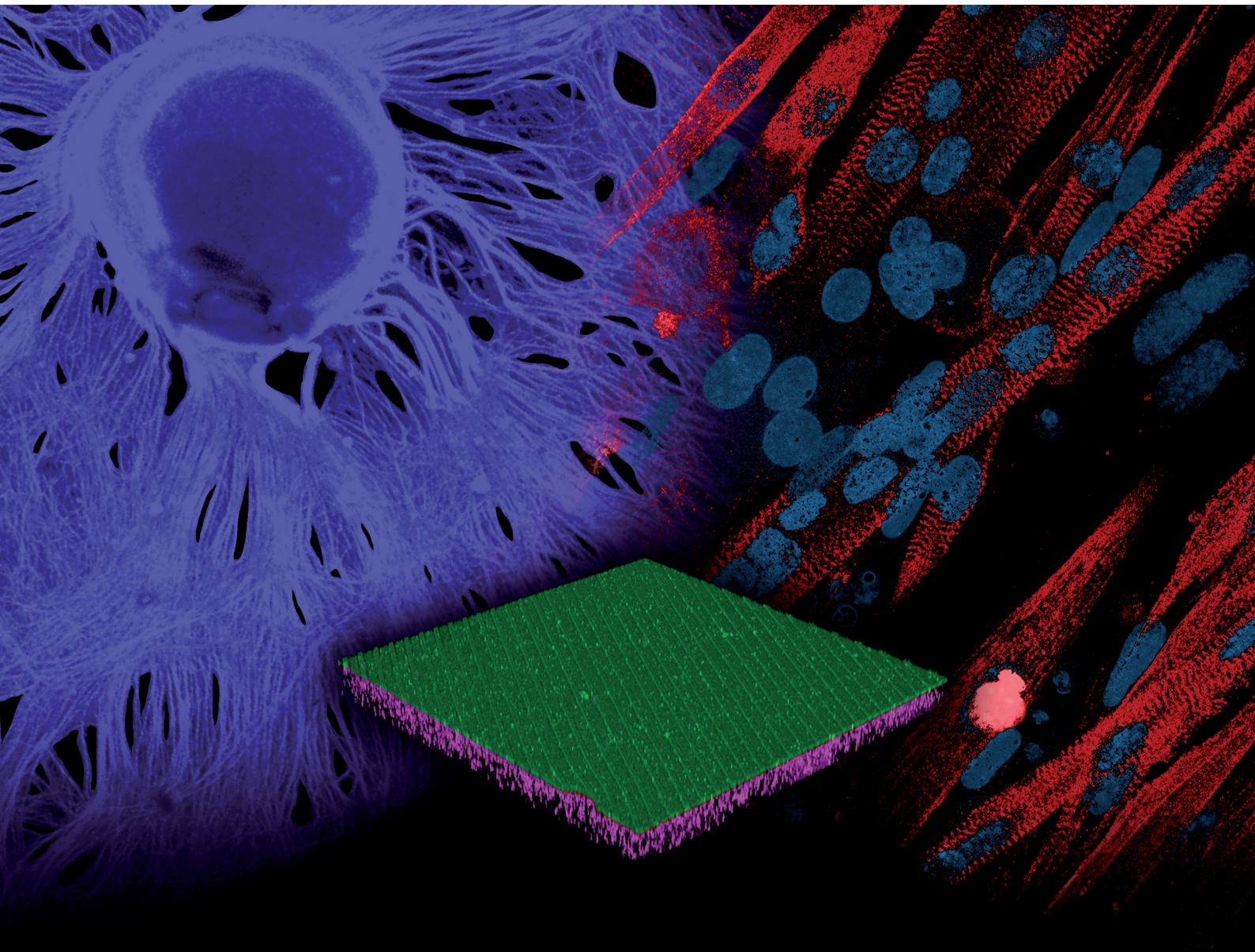


Biomaterials Science

Volume 8
Number 2
21 January 2020
Pages 521-748

rsc.li/biomaterials-science



ISSN 2047-4849




PAPER

Ashutosh Agarwal *et al.*
Enzymatically crosslinked gelatin-laminin hydrogels for
applications in neuromuscular tissue engineering



Cite this: *Biomater. Sci.*, 2020, **8**, 591

Enzymatically crosslinked gelatin–laminin hydrogels for applications in neuromuscular tissue engineering†

Rachel R. Besser,^a Annie C. Bowles,^a Ahmad Alassaf,^{a,b} Daniel Carbonero,^a Isabella Claire,^a Ellery Jones,^a Joseph Reda,^a Laura Wubker,^a Wyndham Batchelor,^a Noël Ziebarth,^a Risset Silvera,^c Aisha Khan,^{c,d} Renata Maciel,^e Mario Saporta^e and Ashutosh Agarwal  *^a

We report a water-soluble and non-toxic method to incorporate additional extracellular matrix proteins into gelatin hydrogels, while obviating the use of chemical crosslinkers such as glutaraldehyde. Gelatin hydrogels were fabricated using a range of gelatin concentrations (4%–10%) that corresponded to elastic moduli of approximately 1 kPa–25 kPa, respectively, a substrate stiffness relevant for multiple cell types. Microbial transglutaminase was then used to enzymatically crosslink a layer of laminin on top of gelatin hydrogels, resulting in 2-component gelatin–laminin hydrogels. Human induced pluripotent stem cell derived spinal spheroids readily adhered and rapidly extended axons on GEL-LN hydrogels. Axons displayed a more mature morphology and superior electrophysiological properties on GEL-LN hydrogels compared to the controls. Schwann cells on GEL-LN hydrogels adhered and proliferated normally, displayed a healthy morphology, and maintained the expression of Schwann cell specific markers. Lastly, skeletal muscle cells on GEL-LN hydrogels achieved long-term culture for up to 28 days without delamination, while expressing higher levels of terminal genes including myosin heavy chain, MyoD, MuSK, and M-cadherin suggesting enhanced maturation potential and myotube formation compared to the controls. Future studies will employ the superior culture outcomes of this hybrid substrate for engineering functional neuromuscular junctions and related organ on a chip applications.

Received 5th September 2019,
Accepted 22nd November 2019

DOI: 10.1039/c9bm01430f

rs.c.li/biomaterials-science

1. Introduction

The extracellular matrix (ECM) plays an instructive role in the development and function of tissues *in vivo*. Hence, a more representative recapitulation of the ECM composition is an important consideration in *in vitro* tissue engineering. In recent years, biomimetic ECM has been engineered to recapitulate the *in vivo* microenvironment including appropriate elastic moduli,^{1,2} pore size,^{3,4} and major ECM proteins.⁵ Two

important ECM components present in most human tissues are collagen and laminin.⁶ While collagen is the most abundant ECM protein, the feasibility for its experimental use may be limited, *e.g.* it is relatively expensive and hydrogel formation can be challenging. As an inexpensive substitute, gelatin hydrogels have been widely used in the culture of skeletal muscle cells,^{7,8} podocytes,⁹ cardiomyocytes,¹⁰ and hepatocytes.³ The basal lamina of these organ systems however, also contains laminin, a high molecular weight protein ECM component, important in cell adherence and migration.^{11–15}

Laminin (LN) coated surfaces have been frequently used to culture neurons and Schwann cells, yet its associated properties such as stiffness and downstream cellular effects have not been fully correlated to native neural ECM.^{16,17} Additionally, laminin has been successfully functionalized to multiple synthetic and biological materials including hyaluronic acid,^{18,19} agarose,²⁰ collagen,²¹ poly(ethylene glycol),²² and polycaprolactone.^{23,24} There is a need for the development of a substrate containing both gelatin and laminin, which can more authentically recapitulate the ECM composition and mechanical properties. Here, a LN-coated gelatin hydrogel demonstrated an improved ECM substrate that closely mimics

^aDepartment of Biomedical Engineering, University of Miami, 1251 Memorial Dr, MEA 203, Coral Gables, FL 33146, USA. E-mail: A.agarwal2@miami.edu; Tel: +1(305) 243-8925

^bDepartment of Medical Equipment Technology, Majmaah University, Al Majmaah 11952, Saudi Arabia

^cMiami Project to Cure Paralysis, University of Miami Miller School of Medicine, 1095 NW 14th Terrace #48, Miami, FL 33136, USA

^dInterdisciplinary Stem Cell Institute, University of Miami Miller School of Medicine, 1600 NW 10th Ave #1140, Miami, FL 33136, USA

^eDepartment of Neurology, University of Miami Miller School of Medicine, 1120 NW 14th St, Suite 1310, Miami, FL 33136, USA

† Electronic supplementary information (ESI) available. See DOI: 10.1039/c9bm01430f

the ECM found in many cell types and, in turn, provided appropriate mechanical cues and characteristics beneficial to multiple cell types.

In this study, we developed a 2-component biomaterial; a gelatin hydrogel crosslinked with laminin using microbial transglutaminase (mTg). mTg is a naturally occurring enzyme, commonly used in the food industry, that catalyzes the formation of covalent *N*-ε-(γ-glutamyl) lysine amide bonds.⁴ These amino acid groups are present in many proteins including gelatin, laminin, fibronectin, and vimentin. The gelatin–laminin (GEL-LN) material is easy to fabricate, since mTg is water-soluble, inexpensive, and highly biocompatible. Additionally, the GEL-LN hydrogel can be micromolded with the desired topography using techniques borrowed from soft lithography.

We first fabricated micromolded gelatin hydrogels using mTg as a crosslinker.^{10,25–27} After the gelatin hydrogel had formed, a laminin layer was enzymatically crosslinked to the top of the gelatin hydrogel using additional mTg.²⁸ Fluorescence microscopy confirmed the presence of a thin layer of laminin on the surface of the 2D gelatin hydrogel. Subsequently, atomic force microscopy (AFM) was used to confirm the maintenance of the micromolded topography after laminin addition. The mechanical properties of the GEL-LN hydrogel were fully characterized using AFM, rheometry, and swelling measurements. We then tested GEL-LN substrates for the culture of 3 cell types: human induced pluripotent stem cell (hiPSC) derived spinal spheroids (SpS), primary rat Schwann cells, and C2C12 skeletal muscle cells. We sought to determine the morphological and functional cellular outcomes for these cell types when cultured on GEL-LN compared to commonly used substrates. SpS were cultured on isotropic GEL-LN hydrogels, and morphological and functional measurements, such as calcium imaging and electrophysiology, were performed. Primary rat Schwann cells were cultured on the GEL-LN hydrogel and assessed for attachment, proliferation, and expression of S100 and P75. C2C12 mouse skeletal muscle cells were cultured on anisotropic micromolded surfaces for up to 28 days without delamination. We examined the morphological changes and protein expression over the 28-day period and compared these outcomes to cultures on a pure gelatin hydrogel. Since neurons, Schwann cells, and skeletal muscle cells form the cellular components of neuromuscular junctions, this platform is ideally suited for the co-culture of these cell lineages for the generation of a functional neuromuscular junction platform. Future studies will also explore the use of mTg to crosslink gelatin hydrogels with additional proteins such as fibronectin and vimentin to create chemically defined ECM scaffolds.

2. Materials and methods

2.1. Hydrogel fabrication

Gelatin hydrogels were fabricated using a previously reported method.¹⁰ Type A porcine gelatin (Sigma, Saint Louis, MO) at

various concentrations (4%, 6%, 8%, 10% w/v) and mTg (4% w/v; Ajinomoto, Tokyo, Japan) were dissolved in deionized water. Once dissolved, the solution was aliquoted (150 μL) onto 18 mm glass coverslips that had been oxidized by exposure to 0.1 M NaOH for 5 minutes, silanized with 0.5% (3-aminopropyl)triethoxysilane (APTES) in 95% ethanol for 5 minutes, and chemically activated by 0.5% glutaraldehyde for 30 minutes.²⁹ Polydimethylsiloxane (PDMS; Electron Microscopy Sciences, Hatfield, PA) stamps were placed on top of the gelatin solution and left overnight at room temperature to crosslink. PDMS stamps were removed from the gelatin hydrogels and the hydrogels were sterilized for 20 minutes under ultraviolet light in a biosafety hood. Laminin (10 μg mL⁻¹; Gibco, Carlsbad, CA) and mTg (4% w/v) solution were added at a 1 : 1 ratio to a parafilm covered surface. The gelatin hydrogel was inverted onto the drop of laminin–mTg solution. Hydrogels were incubated at 37 °C and under 5% CO₂ for 1 hour. Once removed from the incubator, GEL-LN hydrogels were placed in phosphate buffered saline (PBS; Gibco) and stored at 4 °C until use (Fig. 1).

2.2. Characterization of hydrogel

2.2.1. Immunofluorescent staining. Experimental groups were prepared to assess the presence of a chemically linked laminin layer on top of a gelatin hydrogel: gelatin only (control), isotropic GEL-LN, and micromolded GEL-LN (20 μm × 10 μm, grooves and ridges). Fluoro-Max fluorescent microspheres (1 μm, Alexa Fluor 488, Thermo Fisher Scientific, Waltham, MA) were embedded in the gelatin portion of the hydrogel. Subsequently, laminin was added to all groups except the control samples. Each sample was prepared and stored at 4 °C in PBS overnight. Once hydrated, the samples were incubated with rabbit anti-laminin primary antibody (1 : 200; Abcam, ab11575, Cambridge, UK) followed by Alexa Fluor 555-conjugated goat anti-rabbit secondary antibody (1 : 200; Invitrogen, A21428, Carlsbad, CA). Samples were mounted with prolong diamond antifade mounting solution (Invitrogen) onto microscope slides and stored at 4 °C. Z-Stack hydrogel images were acquired using ALS AF software and a Leica SP5 inverted confocal microscope (Leica, Wetzlar, Germany) and 3-dimensional images were rendered using ImageJ software.

2.2.2. Topographical analysis. To assess the topography of the micromolded GEL-LN hydrogels, AFM was employed. Gelatin only and GEL-LN samples were prepared as described above and hydrated in PBS before AFM measurements were performed using a Bruker Dimension 3100D AFM (Bruker, Billerica, MA). An SCM-PIT 0.01–0.025 Ohm cm antimony doped Si cantilever (spring constant 1–5 N m⁻¹, 2.5–2.5 μm tip diameter, Veeco, Plainview, NY) was used in the tapping mode to obtain the height profile of the respective samples. Section views and 3-dimensional contour plots of the topography were rendered using Nanoscope 5.31r1 software (Bruker) with the height analysis tool.

2.2.3. Rheometry. The elastic modulus of the GEL-LN hydrogels (4%, 6%, 8%, 10%) was characterized by oscillatory tests on a HAAKE Rheostress 6000 rheometer (Thermo Fisher

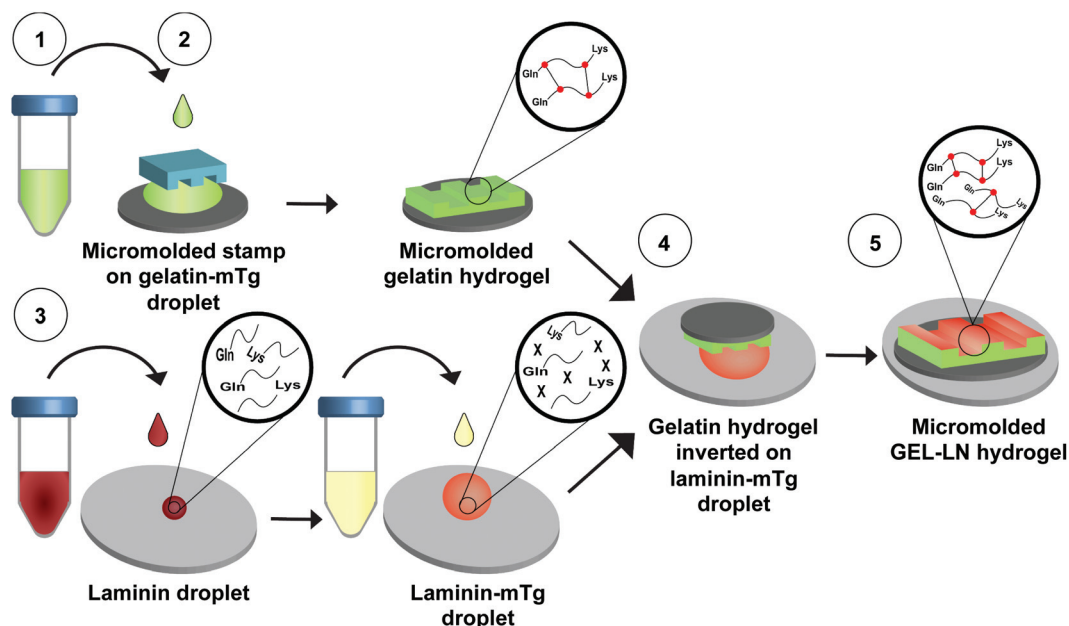


Fig. 1 Schematic showing the GEL-LN fabrication process. (1) Gelatin and mTg are mixed together and added to the top of an activated glass cover slip. (2) The gelatin–mTg mixture is then micromolded under a PDMS stamp and left to cure at room temperature overnight. After curing, the stamp is removed and the gelatin hydrogels are sterilized. (3) A laminin ($10 \mu\text{g mL}^{-1}$) droplet is added to a non-adherent surface (ex: parafilm), after which warm mTg is added to the laminin droplet. (4) Gelatin hydrogel is inverted onto the laminin–mTg droplet. The hydrogel is placed in a 37°C incubator for 1 hour. (5) The GEL-LN hydrogel is removed from the droplet and stored at 4°C in PBS until use.

Scientific). Oscillatory tests (2 total, technical duplicates; $n = 3$ samples) were performed to determine the elastic modulus (E), or stiffness, and the linear viscoelastic region (LVE). The LVE is the region in which measurements are not affected by the magnitude of the shear stress applied. A force-controlled frequency sweep was performed from 1–100 Hz to determine the storage modulus (G') and loss modulus (G'') values. The amplitude of shear stress was held constant at 0.5 N. The elastic modulus (E) was obtained from the storage and loss moduli:

$$G = \sqrt{G'^2 + G''^2} \quad (1)$$

$$E = 2G(1 + \nu) \quad (2)$$

where ν is the Poisson's ratio for hydrogels.^{30,31} To determine the LVE, an amplitude sweep was performed from approximately 0–100% γ values. This test confirmed that the storage and loss moduli obtained from the frequency sweep were within the LVE, and therefore were viable measurements independent of the applied stress.

2.2.4. Atomic force microscopy. To characterize the elastic modulus of the GEL-LN hydrogel, hydrogels were prepared (4%, 6%, 8%, and 10% gelatin w/v) in 35 mm Petri dishes and phenol free medium was added due to the interference of red media with the AFM laser. The dishes were stored at 4°C overnight to allow the hydrogels to reach equilibrium. Each hydrogel was submerged in phenol free media immediately prior to elasticity characterization to preserve hydration. A custom AFM designed for mechanical measurement was used to indent the hydrogels; this AFM design and setup has been described

previously.^{32–34} To microindent the hydrogel, a sphere tipped cantilever (spring constant 0.06 N m^{-1} , $2 \mu\text{m}$ spherical tip diameter, Novascan, Boone, IA) is fixed onto a piezoelectric actuator ($60 \mu\text{m}$ maximal expansion, P-841.40, Physik Instrumente, Germany) and lowered onto the sample at $15 \mu\text{m s}^{-1}$ until the piezoelectric actuator reaches its maximum displacement value (1000 V , corresponding to $\sim 20 \text{ nN}$ of the applied force). As the cantilever indents a sample, it deflects; this resultant deflection is measured as a function of actuator displacement. From these measurements, force–deflection curves can be created and fit to the Hertz model for spherical indenters using a custom MATLAB code to obtain the Young's modulus of elasticity, where the Hertz model is:

$$F = \frac{4E\sqrt{R}}{3(1 - \nu^2)} D^{3/2} \quad (3)$$

In this equation, F is the recorded force, E is the Young's modulus of elasticity, ν is the dimensionless Poisson's ratio, R is the radius of the indenter, and D is the recorded indentation.³⁵ Each gel sample was measured a minimum of 20 times, and each curve fit was graphed and inspected to ensure proper curve fitting before analysis.

2.2.5. Swelling. The swelling behavior of the GEL-LN hydrogel was analyzed using a previously reported method.^{36–38} Hydrogel samples ($n = 10$) were fabricated and measured for each condition. To measure the wet weight (W_e), the hydrogel constructs were weighed after 48 hours in high glucose DMEM GlutaMAX media (Gibco) at 37°C . The samples were dried at room temperature for 7 days to achieve a constant weight,

these values were recorded as the dry weight (W_d). The average mass of the glass coverslips was subtracted from both values. The equilibrium percentage of swelling was calculated as follows:

$$\text{Percent Swelling} = (W_e - W_d)/W_d \times 100 \quad (4)$$

2.3. Culture of SpS

2.3.1. SpS differentiation and maintenance. Human motor neurons were differentiated and purified according to previously published methods.^{17,39} Briefly, fibroblasts were obtained from skin punch biopsies and seeded on gelatin-coated 6-well plates. The fibroblasts were transduced with 4 retroviral vectors expressing SOX2, OCT3/4, KLF4, and C-MYC. After 7 to 10 days hiPSCs were identified and frozen until needed. hiPSCs were cultured until 90–95% confluency and then differentiated into motor neurons for 24 days, which were subsequently purified using magnetic bead sorting based on L1CAM. The purified motor neurons were cultured with agitation until they formed SpS. SpS were seeded onto GEL-LN hydrogels or LN coated surfaces and were maintained in DMEM/F12 GlutaMAX (Thermo Fisher) media containing 0.32% D-glucose (Thermo Fisher), 0.8 mM L-ascorbic acid (Sigma), 2× N-2 supplement (Thermo Fisher), 2× B27 supplement (Thermo Fisher), 1% penicillin/streptomycin (Thermo Fisher), 1.5 μM retinoic acid (Sigma), 10 μM SB431542 (Sigma), 1 μM dosomorphin (Tocris, Bristol, UK), 200 nM SAG (Tocris), 2 ng mL⁻¹ BDNF (Thermo Fisher), 2 ng mL⁻¹ GDNF (Thermo Fisher), and 2 ng mL⁻¹ CNTF (Thermo Fisher).

2.3.2. Calcium imaging. SpS were seeded onto GEL-LN (10% w/v gelatin) hydrogels or LN coated surfaces and allowed to grow for 5 days. Dye solution was prepared by dissolving 50 μg of Oregon Green 488 BAPTA-1 (Sigma) in 25 μL of DMSO and 25 μL of F127 pluronic acid (Sigma). On day 5, cultures were washed with dPBS once and incubated at 37 °C with phenol free DMEM (Gibco) containing 2 μM dye solution for 45 minutes. Since phenol red contributes to autofluorescence, phenol-free medium was used for calcium imaging studies. After incubation, the cells were washed 2× with dPBS and loaded into a live imaging chamber (Warner Instruments, Hamden, CT). Videos were taken using a Nikon Eclipse Ti inverted microscope (Nikon, Tokyo, Japan). First, high glucose phenol free medium (Gibco) was added to neurons and 30 second videos were taken of any spontaneous calcium cycling. Then, phenol free medium containing 1 mM 4-aminopyridine (Sigma) was added to cultures and 2 minute videos were taken of calcium cycling. The videos were analyzed and graphed using MATLAB software. To calculate the signal to noise ratio (SNR), the videos were run through a MATLAB program. Regions of interest were drawn that contained an axon, and that were far away from an axon. For each frame, the intensity of axon-free ROI was subtracted from the intensity of axon-containing ROI ('Signal'). The difference was then divided by the intensity of axon-free ROI ('Noise') to arrive at the SNR of that frame.

2.3.3. Microelectrode array recordings. MEAs (60MEA200/30IR-TI-GR; Multichannel Systems, Reutlingen, Germany) were prepared by either LN coating (10 μg mL⁻¹; $n = 2$) or adding a GEL-LN (10% w/v gelatin) hydrogel ($n = 2$) to the electrode surface in the well. SpS were added inside the MEA well and cells were allowed to adhere and were cultured for 8 days. On days 8 and 13, extracellular electrophysiological recordings were taken using the MEA2100 system with a temperature (37 °C) controller and an interface board that connects the system to a PC (Multichannel Systems). Multichannel experimenter and analyzer software were used to perform on-line recordings and off-line analysis of the data, respectively. Data values were filtered with a high pass filter (200 Hz) and then a low pass filter (4000 Hz) and sampled at 25 kHz. The noise in each channel was determined and a threshold of 10 times the standard deviation of the noise was set to determine a spike. The average number of spikes per active channel, number of bursts per active channel, mean burst duration, interburst interval, and number of spikes in a burst were extrapolated from the recordings. The number of active channels was determined by using a channel with 6 spikes per minute.⁴⁰ A burst was determined using 5 well reported criteria: minimum of 5 spikes, minimum duration of 50 ms, interburst interval of 100 ms, maximum of 50 ms interval to start a burst, and maximum of 50 ms interval to end a burst. The recording file was analyzed additionally using a MATLAB toolbox, provided by Multichannel Systems, to calculate the average spike amplitude of each condition.^{41–44}

2.3.4. Immunocytochemistry. SpS were cultured for up to 21 days and fixed in 4% paraformaldehyde for 20 minutes. To visualize SpS adherence and axonal growth, SpS were incubated with primary antibody chicken/IgY anti-neurofilament light (Thermo Fisher Scientific, PA1-10000; 1 : 2500) overnight at 4 °C followed by a secondary antibody Alexa Fluor 647-conjugated AffiniPure Rabbit anti-chicken IgY (Jackson Immuno Research Laboratories, 303-605-003; 1 : 400). SpS were mounted with prolong diamond antifade mounting solution on microscope slides and stored at 4 °C until imaging.

2.4. Culture of Schwann cells

2.4.1. Schwann cell harvest and culture. Adult female Fischer rats (Harlan Company, Indianapolis, IN) were housed according to NIH guidelines and the Guide for the Care and Use of Animals. All animal procedures employed in this study were approved by the Institutional Animal Care and Use Committee (IACUC) of the University of Miami (IACUC approval # 10-032, dated: 2010). Primary Schwann cells were isolated from a rat using previously described methods approved by the University of Miami Animal Care and Use Committee.⁴⁵ A nerve section was taken from a rat and transported in Belzer UW® Cold Storage Solution (Bridge to Life Ltd, Columbia, SC) and processed within 24 hours. The nerve was dissected under a microscope into fascicles in sterile Leibovitz's medium (Invitrogen) containing gentamicin (40 mg mL⁻¹; Fresenius Kabi Company, Bad Homburg, Germany). Fascicles were cultured at 37 °C for 5–8 days with

Schwann cell growth medium containing $1\times$ Dulbecco's modified Eagle's medium (Life Technologies), 10% fetal bovine serum (Hyclone, GE Healthcare Life Sciences, South Logan, UT), 2 μM forskolin (Sigma-Aldrich), 10 nM human recombinant heregulin $\beta 1$ (Genentech, South San Francisco, CA), 4 mM L-glutamine (Life Technologies), and 0.064 mg mL^{-1} gentamicin (APP Pharmaceutical/Fresenius Kabi USA, Lake Zurich, IL) and subsequently treated with dissociation enzymes (collagenase, 0.5 PZU mL^{-1} , and neutral protease, 2 DMCU mL^{-1} ; Serva, Tulsa, OK) for 16 to 18 hours. The isolated cells (passage 0, P0) were seeded onto LN coated tissue culture flasks and propagated until the cells reached 60–80% confluence and expanded up to passage 3, P3, or cryopreserved with DMSO and stored in liquid nitrogen for long-term banking.

When ready, Schwann cells were thawed and seeded in LN coated flasks and cultured in Schwann cell growth media until confluent. Once the cells were confluent they were lifted from the surface with TrypLE (Thermo Fisher Scientific), counted, and re-suspended in an appropriate amount of media. Cell containing medium was added to isotropic gelatin hydrogels and GEL-LN hydrogels at a density of 25 000 cells per cm^2 and the samples were cultured for 2 days.

2.4.2. Immunocytochemistry. Primary rat Schwann cells were cultured for 2 days and fixed in 4% paraformaldehyde for 10 minutes. To visualize the attachment and morphology of the cells, Schwann cells were incubated with primary antibody polyclonal rabbit anti-S100 (Dako, GA50461-2, Santa Clara, CA) for 30 minutes at room temperature followed by a secondary antibody Alexa Fluor 555 goat anti-rabbit (1:200; Invitrogen, A21428). Schwann cells were mounted with prolong diamond antifade mounting solution on microscope slides and stored at 4 °C until imaging.

2.5. Culture of C2C12 skeletal muscle cells

2.5.1. Long-term culture. Commercially available mouse C2C12 skeletal muscle cells (bought from ATCC, Manassas, VA, catalog# CRL-1772) were seeded on either micromolded (20 $\mu\text{m} \times 10 \mu\text{m}$, grooves and ridges) gelatin (10% w/v) or GEL-LN (10% w/v gelatin) hydrogels and maintained in culture over a period of 35 days. Approximately 25 000 cells per cm^2 were seeded onto each hydrogel in a 12-well plate. The cells were cultured in growth media containing high glucose DMEM GlutaMAX (Gibco), 10% FBS (Gibco), and 1% penicillin–streptomycin, until confluency was achieved. Once confluent, the media were replaced with muscle differentiation media containing high glucose DMEM, 2% horse serum (ATCC), and 1% penicillin–streptomycin. Experimental tests were performed on the specified days within the 35-day culture period.

2.5.2. Immunocytochemistry and flow cytometry. C2C12 skeletal muscle cells were cultured for up to 35 days and subsequently fixed in 4% paraformaldehyde for 15 minutes. To visualize the sarcomeric structure, determine the number of total nuclei, and analyze the myogenic index, C2C12 were incubated with a primary antibody mouse monoclonal anti- α -sarcomeric actinin (1:200; Sigma, A7732) or mouse anti-MHC (1:200; clone A4.1025; EMD Millipore, 05-716,

Burlington, MA) followed by Alexa Fluor 647-conjugated goat anti-mouse secondary antibodies (1:200; Invitrogen, A21237), Phalloidin Alexa Fluor 488 (Invitrogen, A12379) and DAPI (1:200). All cultures were mounted with prolong diamond antifade mounting solution onto microscope slides and stored at 4 °C until imaging.

At 7 days, biological duplicates of C2C12 cells seeded on gelatin or GEL-LN were collected by trypsinization (0.25% trypsin-EDTA; Gibco) and pelleted. Samples were re-suspended in sterile staining buffer containing PBS with bovine serum albumin (0.005%; Sigma-Aldrich) and 1 mM EDTA (pH 7.5; Gibco) and then stained with PE-conjugated anti-mouse ITGA7 (Invitrogen) and Ghost Dye™ Red 780 viability dye (Tonbo Biosciences, San Diego, CA) for 20 minutes at 4 °C. The cells were subsequently washed twice with staining buffer, and 50 000 events were acquired using CytExpert Software with a CytoFLEX C0-B5-R3 Flow Cytometer (Beckman Coulter Life Sciences; Indianapolis, IN) for each sample. Events were analyzed by forward and side-scatter followed by live–dead discrimination and ITGA7 expression of unstained and stained samples using Kaluza v2.1 software (Beckman Coulter Life Sciences). The generated histograms demonstrate the positive ITGA7 expression of duplicates (blue and green lines) based on the gating strategy against the respective unstained controls (red lines) which was quantitatively compared.

2.5.3. Quantitative reverse transcription polymerase chain reaction. C2C12 cell samples seeded onto gelatin or GEL-LN hydrogels were collected during differentiation. At 7 days after the start of differentiation, triplicate samples for each condition were collected by trypsinization, and total RNA was isolated using the RNeasy Plus Kit (Qiagen, Germantown, MD) according to the manufacturer's instructions. RNA (1 μg) for each sample was synthesized into complementary DNA using SuperScript IV VILO Mastermix (Thermo Fisher Scientific). Quantitative reverse transcription polymerase chain reaction (RT-qPCR) was performed for each sample using mouse-specific primers for myogenin, MHC, MyoD, muscle-specific tyrosine kinase (MuSK), LDL receptor related protein-4 (Lrp4), cadherin-2 (CDH2, N-cadherin), cadherin-15 (CDH15, M-cadherin), and glyceraldehyde 3-phosphate dehydrogenase (GAPDH) with sequences previously reported.⁴⁶ Quantitative comparison of each gene expression level for each sample was analyzed by the $\Delta\Delta\text{Ct}$ method, and values for C2C12 samples cultured on GEL-LN were represented as the relative fold change normalized to those cultured on gelatin ($n = 3$).

2.5.4. Morphological analysis. On days 7, 14, 21, 28, and 35, C2C12 cells were fixed and immunostained for MHC ($n = 2$) or α -sarcomeric actinin ($n = 2$) to assess the morphology of the tissue. A Nikon Eclipse Ti inverted microscope was used to take images of the cultures (5 fields of view per slide) and ImageJ was used to analyze the images. To assess total nuclei, the number of nuclei in each field of view was counted. Subsequently, the number of nuclei contained in myotubes positively stained for MHC or α -sarcomeric actinin was counted. The myogenic index was calculated by dividing the number of nuclei contained in myotubes by the number of

total nuclei. Protein levels for MHC and F-actin were quantified by totaling the number of fluorescent pixels in each field of view using ImageJ software (National Institute of Health, Bethesda, MA).

2.6. Statistical analysis

All statistical analysis was performed using Prism v8 software (GraphPad, San Diego, CA). Student's *t*-tests and one-way analysis of variance followed by Tukey's *post hoc* test were used for statistical comparisons. All values were reported as the mean \pm standard error of the mean unless reported otherwise, and $p < 0.05$ was considered statistically significant.

3. Results

3.1. Hydrogel fabrication

mTg is an enzyme commonly used to crosslink gelatin for the formation of gelatin hydrogels. mTg catalyzes the formation of *N*- ϵ -(gamma-glutamyl) lysine amide bonds, which are present in various proteins and ECM components.⁴ While the side reactions catalyzed by reaction intermediates have been recently hypothesized in the pathogenesis of auto-immune disease⁴⁷ and neurological disease,⁴⁸ the enzyme itself or the ammonia side product has not been implicated in any *in vitro* toxicity.

In this study, we used mTg to enzymatically crosslink a thin laminin layer to a 2-dimensional gelatin hydrogel. Initially,

mTg (4% w/v) was added to porcine gelatin (4%, 6%, 8%, and 10% w/v) and subsequently inverted to obtain a homogeneous mixture (Fig. 1). The solution was then added to 18 mm chemically activated glass coverslips, patterned using a polydimethylsiloxane (PDMS) stamp, and allowed to cure overnight. Once the gelatin hydrogel was fully formed, a droplet of laminin ($10 \mu\text{g mL}^{-1}$) and mTg (4% w/v) was added to a parafilm-lined Petri dish and the gelatin hydrogel was inverted onto the laminin-mTg solution (Fig. 1).

To confirm the presence of laminin, fluorescence microscopy was performed, and 3-dimensional renderings of the GEL-LN hydrogels were created (Fig. 2D–F). When preparing samples for imaging, fluorescent microbeads ($1 \mu\text{m}$ diameter) were embedded in the bulk gelatin hydrogel (10% w/v). Fabrication of 3 conditions was performed including an isotropic gelatin only hydrogel (control), an isotropic GEL-LN hydrogel, and a micromolded ($20 \mu\text{m}$ grooves separated by $10 \mu\text{m}$ ridges) GEL-LN hydrogel. All 3 experimental groups were immunostained for laminin and imaged using a confocal Leica SP5 inverted microscope. The control hydrogel only fluoresced in the FITC channel (beads) while no fluorescence in the TRITC channel (laminin) was observed (Fig. 2A and D). Conversely, under both GEL-LN hydrogel conditions, fluorescent beads and a thin laminin layer were visible (Fig. 2B, C and E, F). While the thickness of the laminin layer was not directly measured, it is estimated to be approximately one protein layer thick. Additionally, images obtained for the micromolded GEL-LN hydrogels indicate that the laminin fol-

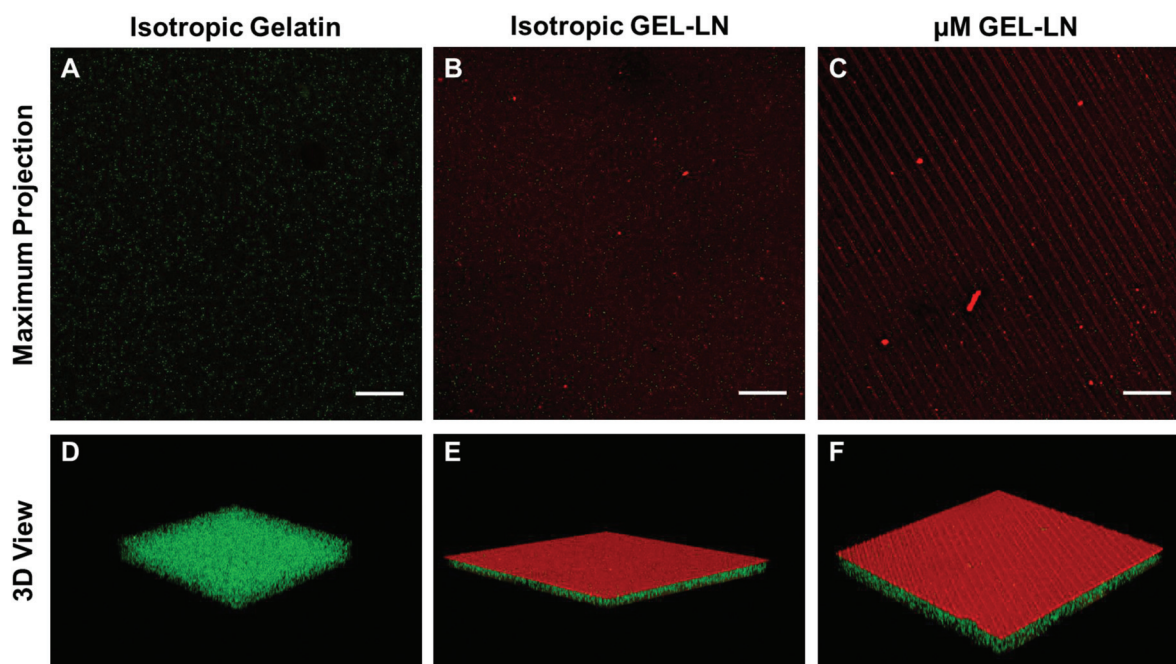


Fig. 2 Fluorescence microscopy visualized and validated each experimental substrate. The gelatin (10% w/v) layer of the hydrogel was embedded with $1 \mu\text{m}$ fluorescent beads (green), and each hydrogel was immunostained for the presence of laminin ($10 \mu\text{g mL}^{-1}$; red). Z-stack images were taken of each experimental group. Three experimental groups were analyzed: (1) isotropic gelatin hydrogel, (2) isotropic GEL-LN hydrogel, and (3) micromolded (μM) GEL-LN hydrogel. (A–C) Maximum projection of z-stack images visualizes the topography of each substrate. Scale bar represents $100 \mu\text{m}$. (D–F) 3D rendered images of z-stack images show protein distribution and patterning of each hydrogel.

lowed the patterning and did not fill the grooves with protein, which would result in a flat surface (Fig. 2C and F).

Hydrogel topography is an important feature for the culture of multiple cell types including skeletal muscle cells,⁷ cardiomyocytes,⁴⁹ neurons,⁵⁰ and podocytes.⁵¹ Adding grooves and ridges to the hydrogel surface will help align the skeletal muscle tissue, aiding in muscle maturation. To confirm that the groove and ridge structure was maintained, the AFM tapping mode was employed to perform an assessment of the surface topography of both control gelatin hydrogel (Fig. 3A–C) and GEL-LN hydrogel (Fig. 3D–F). The resulting section analysis graph shows a height difference along a $90\ \mu\text{m} \times 90\ \mu\text{m}$ section of the hydrogel. The ridge and groove topography of the hydrogel was maintained after the addition of laminin to the hydrogel surface. This indicates that a thin laminin layer was added to the surface while preserving the hydrogel surface topography.

3.2. Characterization of gelatin–laminin hydrogel

GEL-LN hydrogels are biocompatible and have highly tunable mechanical properties. We assessed the bulk elastic moduli, surface elastic moduli, swelling behavior, and degradation of GEL-LN hydrogels. The degradation of the material under sterile conditions was assessed after 3 weeks. Fig. 4A depicts a GEL-LN hydrogel with micromolded features on day 1 of fabrication and day 21 after fabrication. GEL-LN hydrogels were stored in PBS for 21 days and the micromolded features remain with no indication of degradation. Additionally, this experiment was performed in cell culture media and the GEL-LN stability was maintained. The swelling behavior of the

material was characterized by comparing the dry weight and wet weight of the material. The degree of swelling was inversely proportional to the gelatin concentration and ranged from 620% at 4% gelatin to 340% at 10% gelatin (Fig. 4B). The elastic modulus of GEL-LN hydrogels at 4%, 6%, 8%, and 10% (w/v) gelatin and 4% (w/v) mTg was characterized using rheometry and AFM. These techniques are complementary and provide 2 sets of information for the material mechanical properties. AFM will measure the elastic modulus of the material in small areas on the hydrogel surface; however there can be differences in the level of crosslinking occurring in different locations on the surface.⁵² In contrast, rheometry measures the bulk elastic modulus of the hydrogel and any regional differences in crosslinking or stiffness will be lost, allowing the average value to be obtained. The surface elastic modulus ranged from $4.29 \pm 2.35\ \text{kPa}$ to $24.1 \pm 12.9\ \text{kPa}$ (Fig. 4C), while the bulk elastic modulus of the GEL-LN material ranged from $1.46 \pm 0.33\ \text{kPa}$ to $8.40 \pm 0.73\ \text{kPa}$ (Fig. 4D). These values are within the *in vivo* elastic moduli of multiple cellular ECMs including neuronal and muscle tissue. Rheological measurements were performed for gelatin concentrations ranging from 4%–10% (w/v) and mTg concentrations at 2% and 4% (w/v). The measurements were then used to create a 2D-contour plot of the elastic modulus based on the gelatin and mTg concentration (Fig. 4D). Complete rheometry results for 4%, 6%, 8%, and 10% GEL-LN are compiled in ESI Fig. 1–5.†

3.3. Motor neuron culture

hiPSCs were cultured until 90–95% confluent and subsequently differentiated into motor neurons. Magnetic bead

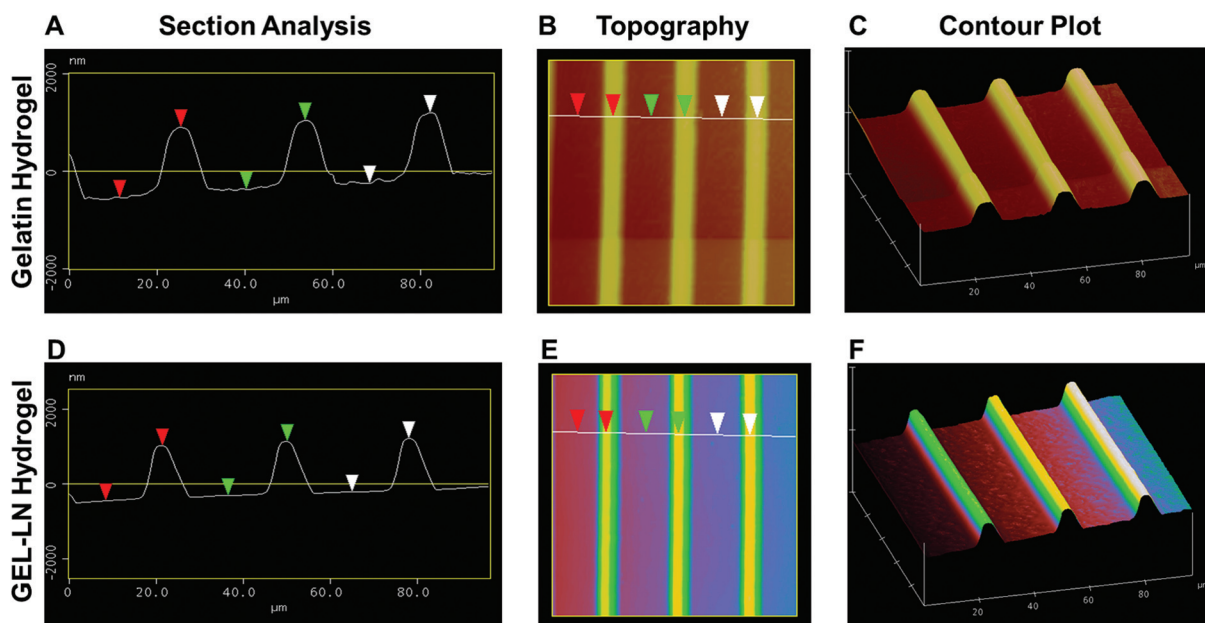


Fig. 3 Surface topography of gelatin and GEL-LN hydrogels was analyzed using atomic force microscopy (AFM). A $90\ \mu\text{m} \times 90\ \mu\text{m}$ section was analyzed in the tapping mode to assess the height differential. Section analysis of $20\ \mu\text{m} \times 10\ \mu\text{m}$ gelatin hydrogel and (D) μm GEL-LN hydrogel. Red, green, and white arrows on section analysis correspond to the arrows on the topography plot. Topography plot of height differences for (B) gelatin and (E) GEL-LN hydrogels. 3D contour plot of μm features on (C) μm gelatin and (F) μm GEL-LN hydrogels.

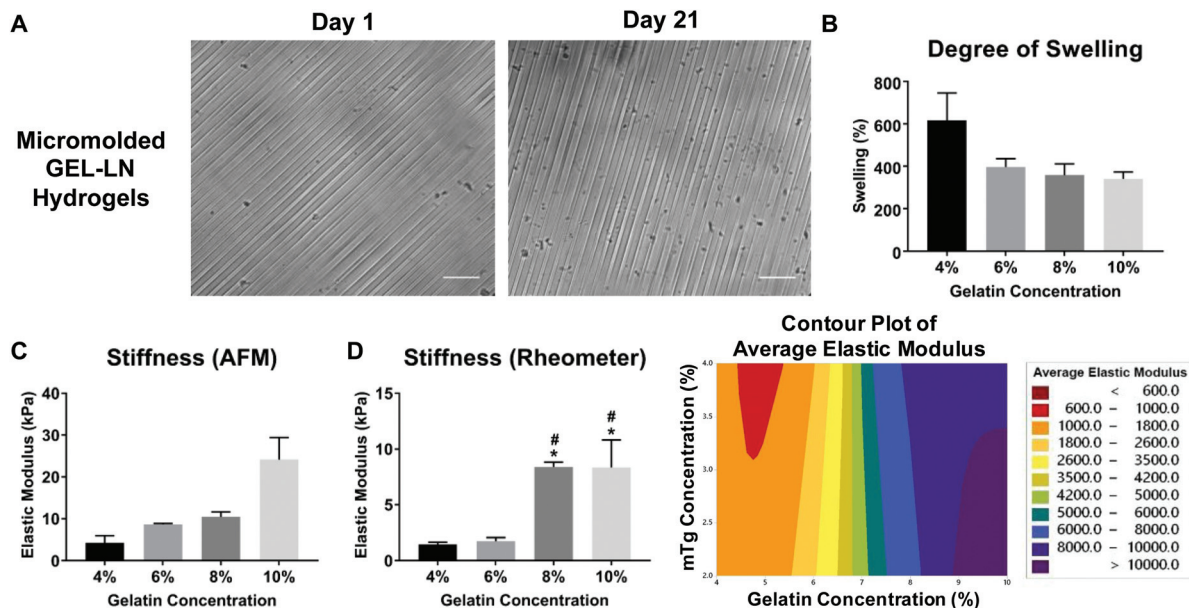


Fig. 4 GEL-LN hydrogels were fabricated with 4% mTg and various gelatin concentrations (4%, 6%, 8%, and 10%). (A) GEL-LN hydrogel was visually assessed at day 1 and day 21 for degradation. (B) Degree of swelling was calculated using dry mass of the hydrogel and wet mass at equilibrium ($n = 10$). (C) The elastic modulus of varying gelatin concentrations was measured with multiple indentations using AFM. (D) GEL-LN hydrogels were fabricated using mTg (2% and 4%) and gelatin (4%, 6%, 8%, and 10%). The elastic modulus was determined with a rheometer and a contour plot was constructed ($n = 3$). Scale bar represents 50 μm . Values represent mean \pm SEM. * $p < 0.05$ compared to 4%; # $p < 0.05$ compared to 6%.

sorting was used to sort iPSC-derived motor neurons and obtain a pure population. iPSC-motor neurons were aggregated to form 3D SpS. SpS were seeded on both isotropic 10% (w/v) gelatin hydrogels and GEL-LN hydrogels (10% w/v) and cultured overnight in neuronal media. After 24 hours, adherence and presence of neural processes were assessed. On the gelatin hydrogel, SpS did not adhere and therefore did not extend any axons (data not shown). Conversely, on GEL-LN hydrogels, SpS readily adhered and started to extend axons after 24 hours (Fig. 5A). The axons continued to grow and increase in density over time (Fig. 5B). After 21 days, SpS were fixed and immunostained for the presence of neurofilament light (NFL) (Fig. 5C). Images showed the positive presence of NFL and axons extended from the SpS body in a radial manner similar to SpS cultured on LN coated surfaces.

The functional characteristics of SpS on LN coated surfaces and GEL-LN hydrogels were assessed by performing calcium imaging and recording electrophysiology. For calcium imaging, SpS were seeded on glass coverslips that were either coated with LN ($n = 2$) or the GEL-LN hydrogel ($n = 2$). After 5 days, the medium was removed, and the cells were stained with Oregon Green 488 BAPTA-1 calcium dye (Fig. 5D and E). Initially, SpS were imaged for 30-second increments for spontaneous signaling. SpS sparking was rare and inconsistent when no stimulation was employed. To induce regular calcium signaling, 1 mM 4-aminopyridine, a potassium channel agonist, was added to the culture media and 2-minute videos were recorded (see ESI Videos 1 and 2† for representative videos of SpS calcium signaling under LN and GEL-LN conditions, respectively). All videos were analyzed using MATLAB program

for signaling (Fig. 5F). On both LN coated surfaces and GEL-LN hydrogels, SpS displayed regular calcium signaling (Fig. 5G). While the number of spikes was similar for both conditions, the intensity of the signaling for SpS on GEL-LN was higher. This increase in intensity could be due to axonal bundling occurring on GEL-LN, leading to thicker axons and therefore increased intensity (Fig. 5E).

SpS were seeded on microelectrode arrays (MEAs) either coated with LN ($n = 2$) or a GEL-LN hydrogel ($n = 2$), the SpS were cultured in neuronal media and recordings were taken on day 8 and day 13 (Fig. 6A and B). Additionally, SpS were seeded on the control gelatin only hydrogels; however recordings were not taken due to the complete absence of cellular adherence. Recordings were taken of spontaneous SpS electrical activity; each recording was 3 minute long and analyzed for spikes, bursts, active channels, burst duration, average amplitude of a spike, mean interburst interval, and number of spikes in a burst (Fig. 6E–K). Representative images of MEA electrical recordings on LN coated surfaces and GEL-LN hydrogels are presented in Fig. 6C and D. There was a significant increase in the number of spikes per active channel ($p < 0.05$) and the number of bursts per active channel ($p = 0.015$) on the GEL-LN hydrogel compared to the LN coated MEA; however the number of active channels remained the same. The average number of spikes in a burst and the mean burst duration remained constant across cultures. The interburst interval, which is the time between bursts, was not statistically longer; however there was an upward trend between the LN coated and GEL-LN conditions. The spike amplitude showed a significant increase for the SpS cultured on the GEL-LN hydrogel ($p < 0.0001$).

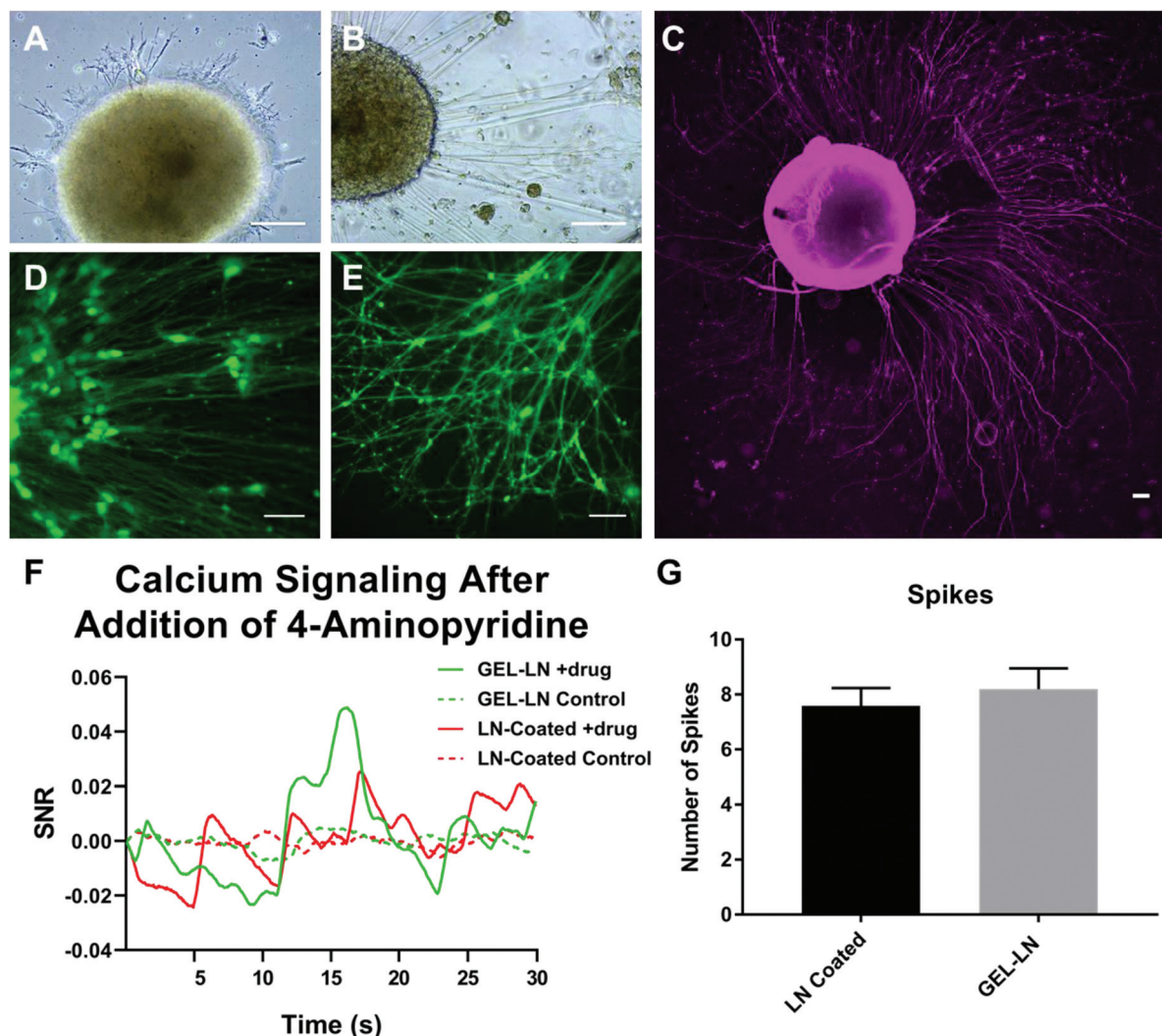


Fig. 5 Visual and functional characterization of SpS cultures. SpS cultured on isotropic 10% (w/v) GEL-LN for (A) 1 day and (B) 21 days show the extension of axonal projections. Scale bar represents 100 μm . (C) SpS were cultured for 21 days and then immunostained for neurofilament light (NFL) to visualize the spatial arrangement of projections. Scale bar represents 100 μm . SpS cultured on (D) a LN coated glass coverslip and (E) GEL-LN hydrogel were stained with Oregon Green 488 BAPTA-1 calcium dye. Scale bar represents 50 μm . (F) Videos were subsequently taken for 30 seconds of unstimulated calcium signaling. 1 mM 4-aminopyridine was added to each condition and 2-minute videos were recorded of calcium signaling. A MATLAB program was used to quantify spiking and graph. (G) Spikes for each stimulated condition were quantitatively compared for SpS cultures. Values represent mean \pm SEM.

3.4. Schwann cell culture

Primary rat Schwann cells were isolated from female rats. The Schwann cells were cultured on a LN coated surface until confluent; the cells were then collected and seeded on isotropic 10% (w/v) gelatin hydrogels and GEL-LN hydrogels (100 000 cells per 18 mm coverslip). The cells were cultured for 2 days and attachment and proliferation were assessed. After 24 hours, the cells adhered to both gelatin and GEL-LN surfaces; however at the 2-day time point many of the Schwann cells cultured on gelatin had detached (Fig. 7A). Conversely, on day 2 of culture the Schwann cells on GEL-LN remained adhered and were present at higher densities (Fig. 7B). On day 2, Schwann cells were fixed and immunostained for S100 and DNA (Fig. 7C–F); 5 images were taken for each condition,

gelatin ($n = 7$) and GEL-LN ($n = 8$). The images were analyzed for total nuclei and S100 positive area. The result showed a significant increase in the number of total nuclei ($p < 0.0001$) and S100 positive area ($p < 0.0001$) for Schwann cells cultured on GEL-LN (Fig. 7G and H). Cell viability and proliferation were assessed for each condition using a live/dead assay and a Click-it EdU assay, respectively. After 2 days of culture, the Schwann cells were alive and proliferating at a rate of approximately 50% on both gelatin hydrogels and GEL-LN hydrogels (ESI Fig. 6[†]).

3.5. Skeletal muscle tissue culture

To assess the ability to culture skeletal muscle tissue long term, C2C12 cells were cultured on micromolded (20 $\mu\text{m} \times$

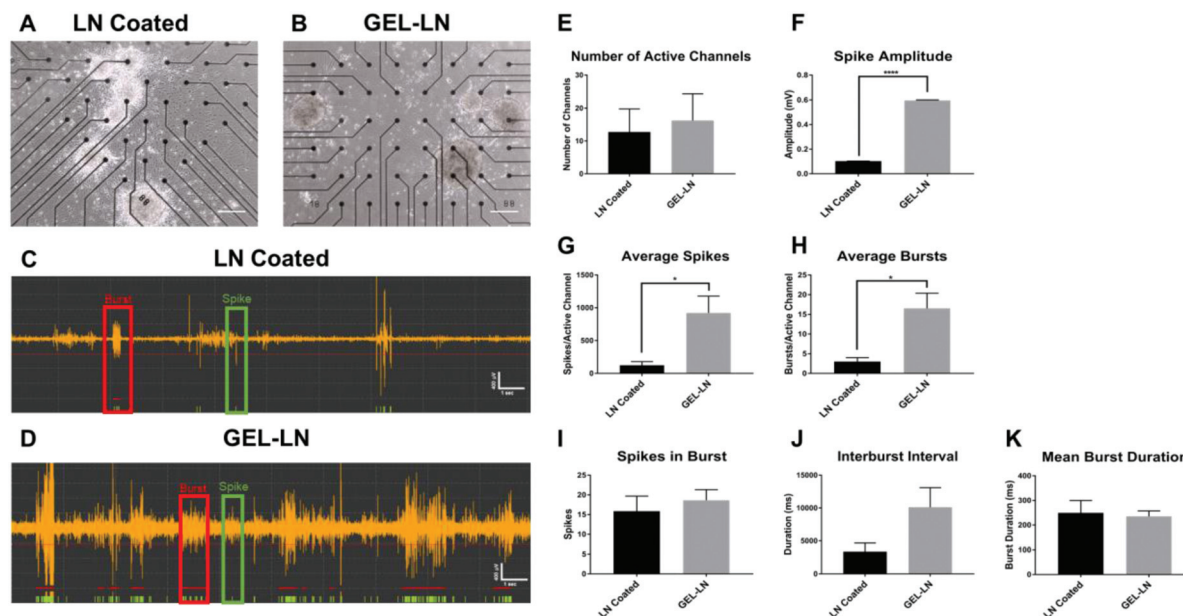


Fig. 6 Substrates promote the distinguishable electrophysiology of SpS cultures. SpS were cultured on (A) LN coated MEAs and (B) isotropic 10% (w/v) GEL-LN hydrogels adhered to MEAs. Scale bar represents 200 μm . Recordings were taken on day 8 and day 13 of culture. Each recording was a total of approximately 3 minutes. 10-second representative image of SpS spiking under a (C) LN coated condition and a (D) GEL-LN condition. (E) Number of average active channels within the conditions. An active channel was designated as any channel with 6 spikes per minute. (F) Average spike amplitude in mV between LN coated and GEL-LN conditions. Average number of (G) spikes and (H) bursts per active channel. (I) Average number of spikes in a burst between LN coated and GEL-LN conditions. (J) Average interburst interval time in milliseconds. Interburst interval is defined as the amount of time between the end of one burst and the beginning of the next. (K) Mean burst duration in milliseconds between LN coated and GEL-LN conditions ($n = 4$ for all experiments). Values represent mean \pm SEM. * $p < 0.05$; **** $p < 0.0001$.

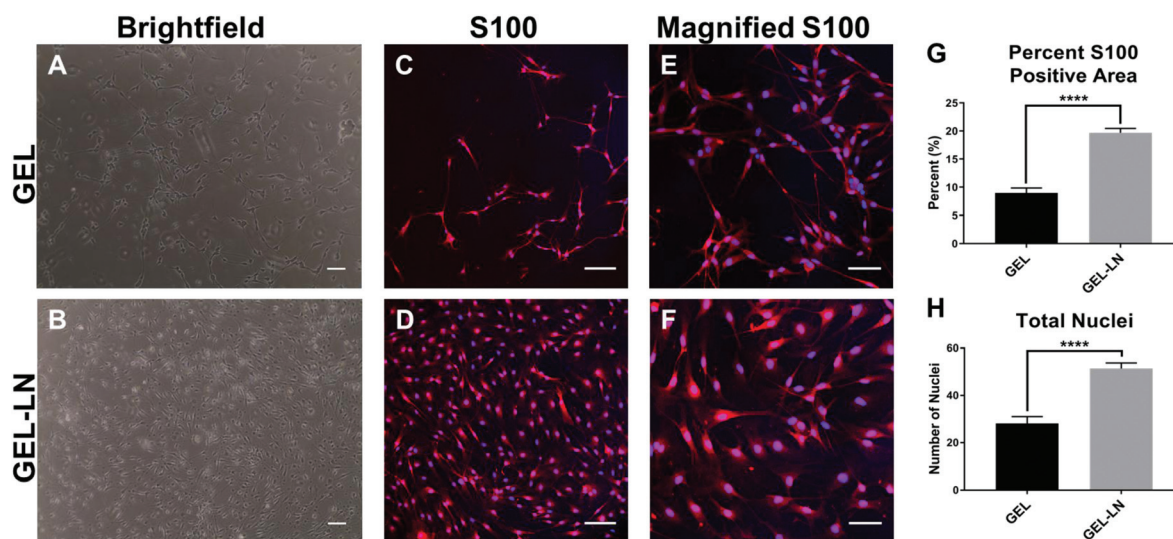


Fig. 7 Characterization of Schwann cell cultures. Schwann cells were cultured on gelatin isotropic 10% (w/v) GEL hydrogels and GEL-LN hydrogels for 2 days. Brightfield image after 48 hours on (A) GEL and (B) GEL-LN. Scale bar represents 100 μm . Fluorescent images of S100 after 48 hours on (C) GEL and (D) GEL-LN. Scale bar represents 100 μm . Magnified views of (C) and (D) on (E) GEL and (F) GEL-LN, respectively. Scale bar represents 50 μm . (G) Quantification of the average percent area of each field of view covered by S100 ($n = 7$ gel, $n = 8$ GEL-LN). (H) Quantification of the average total nuclei in each field of view ($n = 7$ gel, $n = 8$ GEL-LN). Values represent mean \pm SEM. **** $p < 0.0001$.

10 μm , grooves and ridges) GEL-LN hydrogels (10% w/v). Once the cells became confluent, growth medium was replaced with differentiation medium (day 0). The cells were cultured up to

35 days and were fixed on days 7, 14, 21, 28, and 35. The skeletal muscle tissue was then immunostained for myosin heavy chain (MHC; Fig. 8A) or α -sarcomeric actinin (Fig. 8B), F-actin,

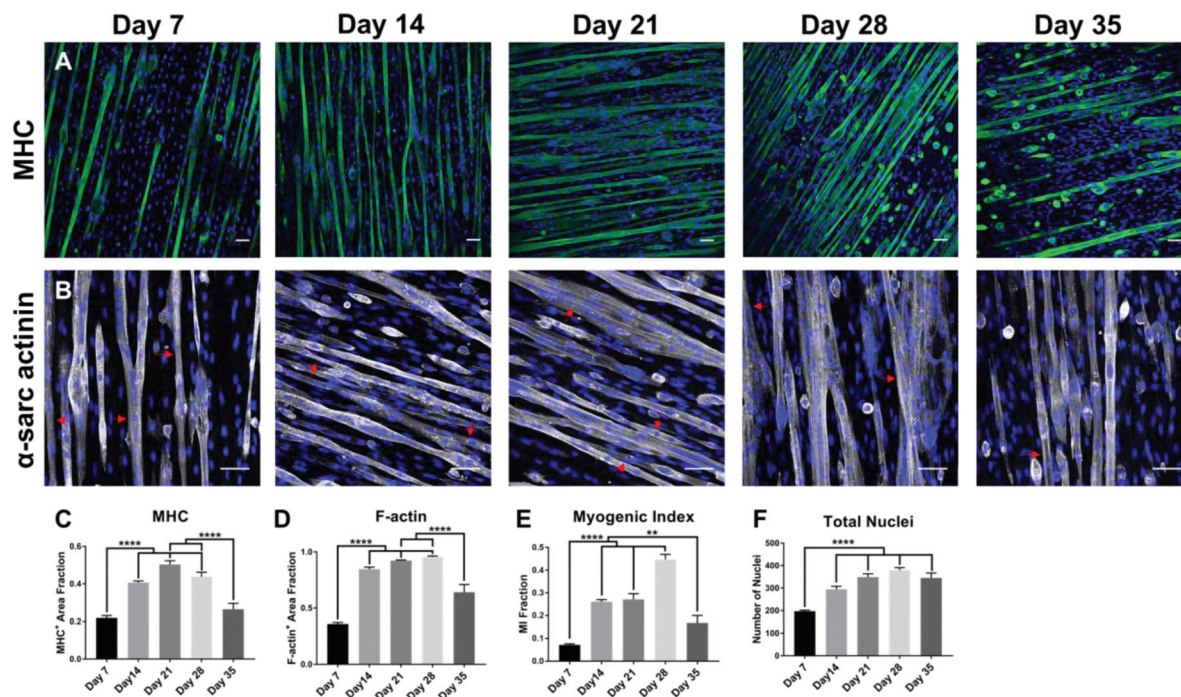


Fig. 8 Analysis of morphology, differentiation, and maturation of skeletal muscle cells cultured on GEL-LN (10% w/v gelatin, 10 $\mu\text{g mL}^{-1}$ laminin). Skeletal muscle cells were cultured up to 35 days and assessed on days 7, 14, 21, 28, and 35. (A) Cells stained for MHC and DNA on days 7–35. Scale bar represents 50 μm . (B) Cells expressing α -sarcomeric actinin on days 7–35. Red arrows indicate organized sarcomeric structures. Scale bar represents 50 μm . (C) A MATLAB program was used to determine the total number of pixels fluorescing for MHC. This number was divided by the total number of pixels to determine the total MHC positive area fraction. Area fraction on day 7 to day 35 is shown. (D) Similarly, total F-actin positive area fraction was quantified. Area fraction on day 7 to day 35 is shown. (E) Myogenic index was determined by assessing the number of nuclei present in MHC positive myotubes and dividing by the total nuclei in the field of view. (F) Total nuclei was counted for each image and day 7 to day 35 were plotted. Values represent mean \pm SEM. ** $p < 0.01$; **** $p < 0.0001$.

and DNA and imaged on a Leica inverted confocal microscope. The cells were analyzed for the positively stained area, myogenic index, and total nuclei. The total MHC positive area fraction increased until day 21 ($p < 0.0001$), then slightly decreased on day 28, and had a significant reduction by day 35 ($p < 0.0001$; Fig. 8C). The total F-actin positive area increased up to day 28 ($p < 0.0001$), and on day 35 there was a significant decrease of F-actin ($p < 0.0001$; Fig. 8D). Similarly, the myogenic index increased significantly until day 28 ($p < 0.0001$), after which there was a significant drop on day 35 ($p < 0.01$; Fig. 8E). The myogenic index on day 35 was still significantly higher than that on day 7 ($p < 0.01$). Lastly, the total nuclei increased until day 28 ($p < 0.0001$) and then plateaued for the rest of the culture period (Fig. 8F). These results indicate that the skeletal muscle tissue can form and remain adherent on GEL-LN for up to 28 days of culture. After 28 days, myoblasts remained present; however there was a delamination phase for differentiated myotubes. To determine if GEL-LN was comparable to gelatin hydrogels, skeletal muscle cells were cultured on gelatin and GEL-LN hydrogels and the myogenic index was calculated over 28 days (ESI Fig. 7A†). Both substrates supported similar muscle differentiation over the 28-day period. Additionally, two geometries were assessed and 20 $\mu\text{m} \times 10 \mu\text{m}$ was used for subsequent experiments (ESI Fig. 7B†).

Skeletal muscle cells were cultured on either micromolded gelatin hydrogels or GEL-LN hydrogels. Cells were seeded and allowed to become 80–90% confluent before they were switched to differentiation medium. On day 7, cells were pelleted and RT-qPCR was performed. Gene expression levels for differentiation and maturation including MHC, MyoD, and myogenin were analyzed. MyoD was significantly upregulated when cultured on GEL-LN (fold 1.60 ± 0.064) compared to gelatin (fold 1.02 ± 0.019 ; $p < 0.001$; Fig. 9A). MHC and myogenin show slight increases in gene expression on day 7 of culture on GEL-LN (Fig. 9B and C). We assessed the expression of genes present in the pathway for acetylcholine receptor (AChR) cluster formation, an important pathway for the formation of neuromuscular junctions. Lrp4 was comparable on gelatin and GEL-LN hydrogels; however MuSK was significantly upregulated for the GEL-LN condition (fold 1.54 ± 0.130 ; $p < 0.05$; Fig. 9D and E). Cell-cell junction markers, N-cadherin (CDH2) and M-cadherin (CDH15), were analyzed. N-Cadherin remained the same across conditions; however M-cadherin was significantly upregulated on GEL-LN (fold 1.26 ± 0.012 ; $p < 0.0001$; Fig. 9F and G). Integrin alpha 7 (ITGA7) is an important protein in the laminin binding mechanism. Flow cytometry was performed on day 7 to assess the percentage of cells which were positive for ITGA7. On GEL-LN, $93 \pm 0.21\%$ of the skeletal

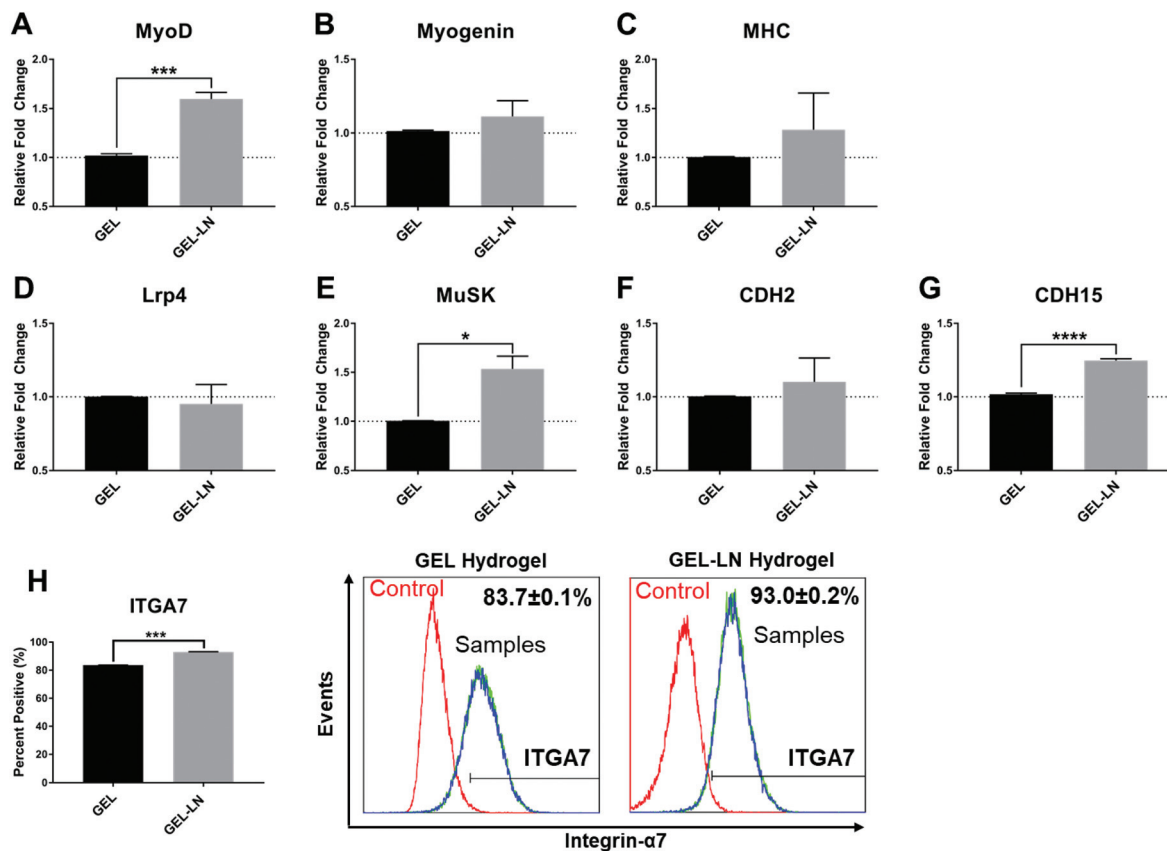


Fig. 9 Skeletal muscle cell gene and protein expression after 7 days of skeletal muscle cell cultures. Gene expression analysis of cells cultured on GEL and GEL-LN was performed and results were plotted for genes active in skeletal muscle differentiation (A) MyoD and (B) myogenin; maturation (C) MHC; acetylcholine signaling pathway (D) Lrp4 and (E) MuSK; and relevant cadherins (F) CDH2 (N-cadherin) and (G) CDH15 (M-cadherin). Values represent mean \pm SEM. * $p < 0.05$, *** $p < 0.001$, **** $p < 0.0001$.

muscle cells were ITGA7 positive, which is a significant increase compared to the gelatin condition ($83.71 \pm 0.09\%$; Fig. 9H).

4. Discussion

4.1. Hydrogel design rationale

Gelatin, which itself is composed of collagen subunits, has been widely implemented as the ECM component in tissue engineering and organ on a chip applications. Gelatin hydrogels are simple to fabricate, easily molded with the desired topography, and considerably low-cost.⁵³ While gelatin has excellent cell-adhesivity and biocompatibility, the ECM of most tissues has a rich composition of many additional proteins. Specifically, laminin and collagen are important ECM components in many human tissues including liver, heart, kidney, muscle, and neuron.^{11–15} Despite the prevalence and pertinence of collagen and laminin, there remains a need for an easy-to-fabricate, affordable material which contains both proteins for an improved ECM substrate.^{54–57}

Several techniques have been evaluated for conjugating proteins to generate hybrid substrates.⁵⁸ A simple and widely used cross-linking method uses chemical reagents to cross-link

aldehyde and amino groups, also known as the Schiff reaction. Glutaraldehyde⁵⁹ is typically used to form strong covalent bonds; however the neurotoxic effects of unreacted glutaraldehyde are well documented.⁶⁰ Another popular bioconjugation technique utilizes *N*-hydroxysulfosuccinimide–carbodiimide chemistry⁶¹ or Michael addition between a nucleophile and a vinyl group^{62,63} requiring multiple steps with control over pH and solvents. Photocrosslinking strategies have also been employed to couple proteins to hydrogels to create biomimetic ECM culture substrates;⁶⁴ however prolonged irradiation and use of a photosensitizer can often lead to local heating and cell damage.⁶⁵ We demonstrate the use of an enzymatic crosslinker, transglutaminase, to not only create thermally stable gelatin hydrogels⁶⁶ with engineered topography and mechanical properties,^{7,10} but to also covalently tether laminin, is significantly more facile than other crosslinking methods to create bioconjugated ECM hydrogels. Furthermore, the 2D nature of this platform allows for the defined architecture of the substrate surface, which would not be possible in a 3D system.^{67,68}

4.2. Matrix stiffness and the effects on neuron maturation

The importance of matrix stiffness for improved neuron differentiation and morphology has been well reported in the

literature.^{69–72} Neural progenitor cells and stem cell derived neurons differentiate and mature more readily on softer substrates compared to stiffer hydrogels or glass surfaces. Furthermore, softer surfaces when compared to glass are less favorable for the differentiation of neural progenitor cells into astrocytes.^{71,73} Here, hiPSC-derived SpS were cultured on GEL-LN hydrogels, which more closely represented the appropriate *in vivo* neural ECM in composition and mechanical properties, improved morphology and electrophysiology outcomes were observed. In future studies, neurons, Schwann cells, and skeletal muscle cells will be cultured together on a single GEL-LN hydrogel. Notably, the average spike amplitude of SpS cultured on GEL-LN was significantly higher than that on the LN coated surface. Habibey *et al.* reported an *in vitro* system which allowed electrophysiology of the neuronal body and axons to be recorded separately revealing a significantly higher amplitude in the axon bundles as compared to the cell body and accompanying singular axons.⁷⁴ Similarly, the thick axonal bundles created on the GEL-LN hydrogel produced higher spike amplitudes in comparison with the notably thinner axons on the LN-coated glass. Additionally, increases in neural spiking and bursting have been linked to neuronal maturation.^{42,75,76} Therefore, the SpS cultured on GEL-LN appear to be more morphologically and functionally mature. Another feature worth noting is that GEL-LN substrates could be stored for up to 21 days before being used for SpS seeding, with no appreciable difference in cell adhesion, indicating that the laminin coating was stable and preserved over that period.

Another attractive feature of the GEL-LN hydrogel is the ability to mold the desired features onto its surface. Surface topography has been shown to enhance neurite length, influence polarity, improve axonal guidance and subsequently increase burst propagation.^{50,77–79} In future studies, GEL-LN will be micromolded with different topographical designs to further enhance axonal growth, help determine burst propagation, and guide axons towards skeletal muscle for neuromuscular junction formation.

4.3. Ideal substrate stiffness for Schwann cells

Schwann cells are commonly cultured on LN coated glass or tissue culture plastic, neither of which properly mimics the composition or elastic modulus of the native ECM. Various types of collagen are the principal molecules of the native Schwann cell ECM, while laminin is an important glycoprotein in the basal lamina.⁸⁰ Laminin has been shown to play an important role in Schwann cell differentiation, proliferation, bipolar morphology, and myelin production.^{80,81} A recent report from Gu *et al.* explored the functional and morphological outcomes of Schwann cells cultured on hydrogels with different elastic moduli.⁸² Substrates with an elastic modulus of 7.45 kPa were suggested to improve the adherence, shape, proliferation, and expression of neurotrophic factors of Schwann cell cultures. Similarly, GEL-LN composed of 10% gelatin possesses an elastic modulus of 8.4 kPa, suggesting that targeting this range of elastic moduli for ECM substrates recapitulates the native *in situ* environment.^{69,83} Here,

Schwann cells cultured on a gelatin only control were proliferative; however, without a laminin component, the cells quickly detached from the substrate indicating the need for laminin for prolonged attachment and proliferation. In future studies, the effect of the appropriate ECM composition in combination with the representative elastic modulus on Schwann cell functional outcomes, such as myelin production and polarity, will be explored.

4.4. Biomimetic ECM composition for the culture of the skeletal muscle tissue

Skeletal muscle cells cultured *in vitro* readily delaminate from commonly used surfaces, such as LN coated glass, after a few days of culture. The ability to culture muscle cells long-term using gelatin hydrogels was recently reported by Bettadapur *et al.*⁷ The reported gelatin hydrogel greatly improved the ability to culture muscle cells over longer periods of time; however the addition of a laminin component could enhance the culture conditions considering the prevalence of laminin in skeletal muscle basal lamina. Accordingly, we cultured skeletal muscle cells on GEL-LN for 28 days without delamination, similar to the gelatin only condition; however improved gene and protein expression was observed on the GEL-LN substrate. ITGA7 is a laminin binding integrin that stabilizes muscle to the underlying matrix.^{84–87} Muscle cells cultured on GEL-LN had significantly more ITGA7 expressing cells when compared to the gelatin only control, indicating a more stable attachment to the underlying substrate. MyoD, myogenin, and M-cadherin are genes active in muscle differentiation.^{88–92} By day 7, MyoD and M-cadherin were significantly upregulated on GEL-LN substrates, indicating enhanced differentiation potential. MHC, a gene corresponding to muscle maturation, was also upregulated after 7 days on GEL-LN, and confocal imaging revealed high protein expression over a period of 35 days.⁴⁶ Taken together, these results indicate that the properties of the GEL-LN substrate greatly improve the maturation and differentiation of skeletal muscle cells. Furthermore, laminin is integral to the formation of AChR clustering on the skeletal muscle membrane.^{93,94} Another important component of the AChR clustering pathways is MuSK, which binds agrin and induces clustering on the muscle membrane. When skeletal muscle cells were cultured on GEL-LN, MuSK expression was significantly upregulated compared to muscle cells cultured on gelatin hydrogels. Increased MuSK expression is suggested to facilitate more AChR clusters on muscle cells cultured on GEL-LN, and therefore improve the formation of functional neuromuscular junctions.

Collectively, our study demonstrates the significance of integrating and diversifying proteins in efforts to engineer improved *in vitro* substrates. The implications of this study are geared to generating ideal platforms of multicellular tissues to study diseases and recapitulate *in situ* mechanisms such as functional neuromuscular junction formation. SpS generated enhanced electrophysiological properties and improved the morphology, Schwann cells improved attachment, and skeletal muscle cells significantly upregulated genes associated with

AChR formation. Both SpS and muscle cells adhered to the substrate readily and were cultured for over 3 weeks, indicating that these cells could be combined in a co-culture system for an extended time period, increasing neuromuscular junction formation and maturation. The technique used in this manuscript could be adapted to utilizing other ECM components, such as fibronectin and vimentin, on gelatin or any protein-based hydrogel, making it a useful technique to fabricate biomimetic hydrogels for numerous cell types.

5. Conclusions

In summary, we describe the use of a naturally occurring and water soluble enzyme, microbial transglutaminase, to fabricate a new biomimetic hydrogel containing gelatin and laminin. GEL-LN hydrogels were engineered in a range of elastic moduli, and maintained their topography after laminin coating, a feature important for recapitulating a native environment as cells respond to topographical cues. Multiple cell types were cultured on the GEL-LN material including hiPSC-derived SpS, Schwann cells, and skeletal muscle cells. GEL-LN was determined to be superior to commonly used substrates such as gelatin hydrogels or LN coated glass. While these selected cells cultured on GEL-LN hydrogels are implicated for generating a functional neuromuscular junction platform, the mTg crosslinking scheme itself can be extended to cross-linking other ECM motifs to gelatin hydrogels.

Funding

This work was supported by the Wallace H. Coulter Center Translational Research Commercialization Grant (AA), the NIH (1UC4DK104208 and 1U01CA233363 to AA), the Mentored Translational Research Scholars Program Award (KL2TR002737) by Miami CTSI (MS), and a Charcot-Marie-Tooth Association research grant (MS).

Conflicts of interest

There are no conflicts to declare.

Acknowledgements

We are grateful for the technical assistance provided by the Dr David F. Meaney lab, and helpful discussions with Dr William Silverman.

References

- 1 A. J. Engler, S. Sen, H. L. Sweeney and D. E. Discher, *Cell*, 2006, **126**, 677–689.
- 2 F. Guilak, D. M. Cohen, B. T. Estes, J. M. Gimble, W. Liedtke and C. S. Chen, *Cell Stem Cell*, 2009, **5**, 17–26.
- 3 R. Gauvin, Y. C. Chen, J. W. Lee, P. Soman, P. Zorlutuna, J. W. Nichol, H. Bae, S. Chen and A. Khademhosseini, *Biomaterials*, 2012, **33**, 3824–3834.
- 4 M. De Colli, M. Massimi, A. Barbetta, B. Di Rosario, S. Nardecchia, L. C. Devirgiliis and M. Dentini, *Biomed. Mater.*, 2012, **7**, 055005.
- 5 S. Hinds, W. Bian, R. G. Dennis and N. Bursac, *Biomaterials*, 2011, **32**, 3575–3583.
- 6 F. T. Bosman and I. Stamenkovic, *J. Pathol.*, 2003, **200**, 423–428.
- 7 A. Bettadapur, G. C. Suh, N. A. Geisse, E. R. Wang, C. Hua, H. A. Huber, A. A. Viscio, J. Y. Kim, J. B. Strickland and M. L. McCain, *Sci. Rep.*, 2016, **6**, 28855.
- 8 L. T. Denes, L. A. Riley, J. R. Mijares, J. D. Arboleda, K. McKee, K. A. Esser and E. T. Wang, *Skeletal Muscle*, 2019, **9**, 17.
- 9 M. Hu, E. U. Azeloglu, A. Ron, K.-H. Tran-Ba, R. C. Calizo, I. Tavassoly, S. Bhattacharya, G. Jayaraman, Y. Chen and V. Rabinovich, *Sci. Rep.*, 2017, **7**, 43934.
- 10 M. L. McCain, A. Agarwal, H. W. Nesmith, A. P. Nesmith and K. K. Parker, *Biomaterials*, 2014, **35**, 5462–5471.
- 11 W. Yang, Q. Chen, R. Xia, Y. Zhang, L. Shuai, J. Lai, X. You, Y. Jiang, P. Bie, L. Zhang, H. Zhang and L. Bai, *Biomaterials*, 2018, **177**, 52–66.
- 12 K. Cameron, R. Tan, W. Schmidt-Heck, G. Campos, M. J. Lyall, Y. Wang, B. Lucendo-Villarín, D. Szkolnicka, N. Bates, S. J. Kimber, J. G. Hengstler, P. Godoy, S. J. Forbes and D. C. Hay, *Stem Cell Rep.*, 2015, **5**, 1250–1262.
- 13 M. A. Horn and A. W. Trafford, *J. Mol. Cell Cardiol.*, 2016, **93**, 175–185.
- 14 L. Sorokin, *J. Cell Biol.*, 1990, **111**, 1265–1273.
- 15 J. Holmberg and M. Durbeek, *Cell Adhes. Migr.*, 2013, **7**, 111–121.
- 16 S. S. Rao and J. O. Winter, *Front. Neuroeng.*, 2009, **2**, 6.
- 17 M. A. Saporta, V. Dang, D. Volfson, B. Zou, X. S. Xie, A. Adebola, R. K. Liem, M. Shy and J. T. Dimos, *Exp. Neurol.*, 2015, **263**, 190–199.
- 18 C. P. Addington, J. M. Heffernan, C. S. Millar-Haskell, E. W. Tucker, R. W. Sirianni and S. E. Stabenfeldt, *Biomaterials*, 2015, **72**, 11–19.
- 19 S. Hou, Q. Xu, W. Tian, F. Cui, Q. Cai, J. Ma and I. S. Lee, *J. Neurosci. Methods*, 2005, **148**, 60–70.
- 20 X. Yu, G. P. Dillon and R. V. Bellamkonda, *Tissue Eng.*, 1999, **5**(4), 291–304.
- 21 S. A. Geissler, A. L. Sabin, R. R. Besser, O. M. Gooden, B. D. Shirk, Q. M. Nguyen, Z. Z. Khaing and C. E. Schmidt, *J. Neural. Eng.*, 2018, **15**, 025004.
- 22 A. T. Francisco, P. Y. Hwang, C. G. Jeong, L. Jing, J. Chen and L. A. Setton, *Acta Biomater.*, 2014, **10**, 1102–1111.
- 23 H. Bahrami, S. H. Keshel, A. J. Chari and E. Biazar, *Artif. Cells, Nanomed., Biotechnol.*, 2016, **44**, 1556–1560.
- 24 M. A. Sahebalzamani, M. T. Khorasani and M. D. Joupari, *Nano Biomed. Eng.*, 2017, **9**(3), 191–198.

- 25 N. Z. Alarake, P. Frohberg, T. Groth and M. Pietzsch, *Int. J. Artif. Organs*, 2017, **40**, 159–168.
- 26 C.-C. Tsai, Y.-J. Hong, R. J. Lee, N.-C. Cheng and J. Yu, *J. Mater. Chem. B*, 2019, **7**, 1064–1075.
- 27 H. Long, K. Ma, Z. Xiao, X. Ren and G. Yang, *PeerJ*, 2017, **5**, e3665.
- 28 G. Damodaran, R. Collighan, M. Griffin and A. Pandit, *J. Biomed. Mater. Res., Part A*, 2009, **89**, 1001–1010.
- 29 P. L. Kuo, H. Lee, M. A. Bray, N. A. Geisse, Y. T. Huang, W. J. Adams, S. P. Sheehy and K. K. Parker, *Am. J. Pathol.*, 2012, **181**, 2030–2037.
- 30 M. Ahearne, Y. Yang, A. J. El Haj, K. Y. Then and K.-K. Liu, *J. R. Soc., Interface*, 2005, **2**, 455–463.
- 31 A. M. Kloxin, C. J. Kloxin, C. N. Bowman and K. S. Anseth, *Adv. Mater.*, 2010, **22**, 3484–3494.
- 32 J. Dias, V. F. Diakonis, V. P. Kankariya, S. H. Yoo and N. M. Ziebarth, *Exp. Eye Res.*, 2013, **116**, 58–62.
- 33 J. Dias, V. F. Diakonis, M. Lorenzo, F. Gonzalez, K. Porras, S. Douglas, M. Avila, S. H. Yoo and N. M. Ziebarth, *Exp. Eye Res.*, 2015, **138**, 1–5.
- 34 E. P. W. Noel, M. Ziebarth, F. Manns, V. T. Moy and J.-M. Parel, *Mol. Vision*, 2007, **13**, 504–510.
- 35 H. Hertz, *Miscellaneous papers*, 1896, ch. 5, p. 146.
- 36 Q. Xing, K. Yates, C. Vogt, Z. Qian, M. C. Frost and F. Zhao, *Sci. Rep.*, 2014, **4**, 4706.
- 37 J. L. Young and A. J. Engler, *Biomaterials*, 2011, **32**, 1002–1009.
- 38 A. Bettadapur, G. C. Suh, N. A. Geisse, E. R. Wang, C. Hua, H. A. Huber, A. A. Viscio, J. Y. Kim, J. B. Strickland and M. L. McCain, *Sci. Rep.*, 2016, **6**, 28855.
- 39 R. Maciel, D. M. Bis, A. P. Rebelo, C. Saghira, S. Züchner and M. A. Saporta, *Exp. Neurol.*, 2018, **307**, 155–163.
- 40 M. Mayer, O. Arrizabalaga, F. Lieb, M. Ciba, S. Ritter and C. Thielemann, *Biosens. Bioelectron.*, 2018, **100**, 462–468.
- 41 E. Cotterill, P. Charlesworth, C. W. Thomas, O. Paulsen and S. J. Eglén, *J. Neurophysiol.*, 2016, **116**, 306–321.
- 42 D. J. Bakkum, M. Radivojevic, U. Frey, F. Franke, A. Hierlemann and H. Takahashi, *Front. Comput. Neurosci.*, 2013, **7**, 193.
- 43 V. Pasquale, S. Martinoia and M. Chiappalone, *J. Comput. Neurosci.*, 2010, **29**, 213–229.
- 44 M. E. J. Obien, K. Deligkaris, T. Bullmann, D. J. Bakkum and U. Frey, *Front. Neurosci.*, 2015, **8**, 423.
- 45 J. Bastidas, G. Athauda, G. De La Cruz, W. M. Chan, R. Golshani, Y. Berrocal, M. Henao, A. Lalwani, C. Mannoji and M. Assi, *Glia*, 2017, **65**, 1278–1301.
- 46 C. L. Happe, K. P. Tenerelli, A. K. Gromova, F. Kolb and A. J. Engler, *Mol. Biol. Cell*, 2017, **28**, 1950–1958.
- 47 B. Fleckenstein, S. W. Qiao, M. R. Larsen, G. Jung, P. Roepstorff and L. M. Sollid, *J. Biol. Chem.*, 2004, **279**, 17607–17616.
- 48 A. Martin, G. De Vivo and V. Gentile, *Int. J. Alzheimer's Dis.*, 2011, **2011**, 865432.
- 49 A. W. Feinberg, P. W. Alford, H. Jin, C. M. Ripplinger, A. A. Werdich, S. P. Sheehy, A. Grosberg and K. K. Parker, *Biomaterials*, 2012, **33**, 5732–5741.
- 50 A. Rajniecek, S. Britland and C. McCaig, *J. Cell Sci.*, 1997, **110**, 2905–2913.
- 51 M. MacGregor-Ramiasa, I. Hopp, A. Bachhuka, P. Murray and K. Vasilev, *Acta Biomater.*, 2017, **56**, 171–180.
- 52 J. A. Last, P. Russell, P. F. Nealey and C. J. Murphy, *Invest. Ophthalmol. Visual Sci.*, 2010, **51**, 6083–6094.
- 53 V. Crescenzi, A. Francescangeli and A. Taglienti, *Biomacromolecules*, 2002, **3**, 1384–1391.
- 54 C. P. Addington, S. Dharmawaj, J. M. Heffernan, R. W. Sirianni and S. E. Stabenfeldt, *Matrix Biol.*, 2017, **60–61**, 206–216.
- 55 A. T. Francisco, R. J. Mancino, R. D. Bowles, J. M. Brunger, D. M. Tainter, Y. T. Chen, W. J. Richardson, F. Guilak and L. A. Setton, *Biomaterials*, 2013, **34**, 7381–7388.
- 56 M. Marcinczyk, H. Elmashhady, M. Talovic, A. Dunn, F. Bugis and K. Garg, *Biomaterials*, 2017, **141**, 233–242.
- 57 A. Farrukh, F. Ortega, W. Q. Fan, N. Marichal, J. I. Paez, B. Berninger, A. del Campo and M. J. Salierno, *Stem Cell Rep.*, 2017, **9**, 1432–1440.
- 58 W. E. Hennink and C. F. van Nostrum, *Adv. Drug Delivery Rev.*, 2012, **64**, 223–236.
- 59 H. F. Liang, M. H. Hong, R. M. Ho, C. K. Chung, Y. H. Lin, C. H. Chen and H. W. Sung, *Biomacromolecules*, 2004, **5**, 1917–1925.
- 60 W. S. Shim, J. H. Kim, K. Kim, Y. S. Kim, R. W. Park, I. S. Kim, I. C. Kwon and D. S. Lee, *Int. J. Pharm.*, 2007, **331**, 11–18.
- 61 A. Agarwal, Y. Farouz, A. P. Nesmith, L. F. Deravi, M. L. McCain and K. K. Parker, *Adv. Funct. Mater.*, 2013, **23**, 3738–3746.
- 62 C. Hiemstra, L. J. van der Aa, Z. Y. Zhong, P. J. Dijkstra and J. Feijen, *Macromolecules*, 2007, **40**, 1165–1173.
- 63 M. Guvendiren and J. A. Burdick, *Nat. Commun.*, 2012, **3**, 792.
- 64 P. A. Levett, F. P. W. Melchels, K. Schrobback, D. W. Hutmacher, J. Malda and T. J. Klein, *Acta Biomater.*, 2014, **10**, 214–223.
- 65 J. Lukaszczyk, M. Smiga, K. Jaszcz, H. J. P. Adler, E. Jahne and M. Kaczmarek, *Macromol. Biosci.*, 2005, **5**, 64–69.
- 66 L. S. M. Teixeira, J. Feijen, C. A. van Blitterswijk, P. J. Dijkstra and M. Karperien, *Biomaterials*, 2012, **33**, 1281–1290.
- 67 Y. Morimoto, M. Kato-Negishi, H. Onoe and S. Takeuchi, *Biomaterials*, 2013, **34**(37), 9413–9419.
- 68 T. A. Dixon, E. Cohen, D. M. Cairns, M. Rodriguez, J. Mathews, R. R. Jose and D. L. Kaplan, *Tissue Eng., Part C*, 2018, **24**(6), 346–359.
- 69 S. K. Seidlits, Z. Z. Khaing, R. R. Petersen, J. D. Nickels, J. E. Vanscoy, J. B. Shear and C. E. Schmidt, *Biomaterials*, 2010, **31**, 3930–3940.
- 70 A. I. Teixeira, S. Ilkhanizadeh, J. A. Wigenius, J. K. Duckworth, O. Inganas and O. Hermanson, *Biomaterials*, 2009, **30**, 4567–4572.
- 71 L. A. Flanagan, Y.-E. Ju, B. Marg, M. Osterfield and P. A. Janmey, *NeuroReport*, 2002, **13**, 2411.

- 72 A. Banerjee, M. Arha, S. Choudhary, R. S. Ashton, S. R. Bhatia, D. V. Schaffer and R. S. Kane, *Biomaterials*, 2009, **30**, 4695–4699.
- 73 P. C. Georges, W. J. Miller, D. F. Meaney, E. S. Sawyer and P. A. Janmey, *Biophys. J.*, 2006, **90**, 3012–3018.
- 74 R. Habibey, A. Golabchi, S. Latifi, F. Difato and A. Blau, *Lab Chip*, 2015, **15**, 4578–4590.
- 75 E. Biffi, G. Regalia, A. Menegon, G. Ferrigno and A. Pedrocchi, *PLoS One*, 2013, **8**, e83899.
- 76 T. Paavilainen, A. Pelkonen, M. E. Makinen, M. Peltola, H. Huhtala, D. Fayuk and S. Narkilahti, *Stem Cell Res.*, 2018, **27**, 151–161.
- 77 N. M. Dowell-Mesfin, M. A. Abdul-Karim, A. M. Turner, S. Schanz, H. G. Craighead, B. Roysam, J. N. Turner and W. Shain, *J. Neural. Eng.*, 2004, **1**, 78–90.
- 78 J. N. Hanson, M. J. Motala, M. L. Heien, M. Gillette, J. Sweedler and R. G. Nuzzo, *Lab Chip*, 2009, **9**, 122–131.
- 79 L. Pan, S. Alagapan, E. Franca, G. J. Brewer and B. C. Wheeler, *J. Neural. Eng.*, 2011, **8**, 046031.
- 80 M. Chernousov and D. Carey, *Histol. Histopathol.*, 2000, **15**, 593–601.
- 81 W. M. Yu, Z. L. Chen, A. J. North and S. Strickland, *J. Cell Sci.*, 2009, **122**, 929–936.
- 82 Y. Gu, Y. Ji, Y. Zhao, Y. Liu, F. Ding, X. Gu and Y. Yang, *Biomaterials*, 2012, **33**, 6672–6681.
- 83 A. Bakshi, O. Fisher, T. Dagci, B. T. Himes, I. Fischer and A. Lowman, *J. Neurosurg.*, 2004, **1**, 322–329.
- 84 J. A. Doe, R. D. Wuebbles, E. T. Allred, J. E. Rooney, M. Elorza and D. J. Burkin, *J. Cell Sci.*, 2011, **124**, 2287–2297.
- 85 H. Colognato, D. A. Winkelmann and P. D. Yurchenco, *J. Cell Biol.*, 1999, **145**, 619–631.
- 86 J. E. Rooney, P. B. Gurpur and D. J. Burkin, *Proc. Natl. Acad. Sci. U. S. A.*, 2009, **106**, 7991–7996.
- 87 D. J. Burkin and S. J. Kaufman, *Cell Tissue Res.*, 1999, **296**, 183–190.
- 88 R. Eftimie, H. R. Brenner and A. Buonanno, *Proc. Natl. Acad. Sci. U. S. A.*, 1991, **88**, 1349–1353.
- 89 M. Juhas, G. C. Engelmayr Jr., A. N. Fontanella, G. M. Palmer and N. Bursac, *Proc. Natl. Acad. Sci. U. S. A.*, 2014, **111**, 5508–5513.
- 90 S. Li, M. P. Czubryt, J. McAnally, R. Bassel-Duby, J. A. Richardson, F. F. Wiebel, A. Nordheim and E. N. Olson, *Proc. Natl. Acad. Sci. U. S. A.*, 2005, **102**, 1082–1087.
- 91 Y. S. Choi, L. G. Vincent, A. R. Lee, M. K. Dobke and A. J. Engler, *Biomaterials*, 2012, **33**, 2482–2491.
- 92 M. Donalies, M. Cramer, M. Ringwald and A. Starzinski-Powitz, *Proc. Natl. Acad. Sci. U. S. A.*, 1991, **88**, 8024–8028.
- 93 J. Sugiyama, D. Glass, G. Yancopoulos and Z. Hall, *J. Cell Biol.*, 1997, **139**, 181–191.
- 94 Z. Vogel, C. N. Christian, M. Vigny, H. Bauer, P. Sonderegger and M. P. Daniels, *J. Neurosci.*, 1983, **3**, 1058–1068.